5. Calibration and Monitoring

R. Snel[1], G. Lichtenberg[2], S. Noël[3], M. Krijger[1], S. Slijkhuis[2], K. Bramstedt[3]

[1] SRON, Netherlands Institute for Space Research, Sorbonnelaan 2, 3584 CA Utrecht, The Netherlands
[2] Remote Sensing Technology Institute, German Aerospace Center (DLR-IMF), Oberpfaffenhofen, 82234 Wessling, Germany
[3] Institute of Environmental Physics / Institute of Remote Sensing (IUP-IFE), University of Bremen, Otto-Hahn-Allee 1, 28359 Bremen, Germany

Abstract: Spaceborne spectral measurements over long time periods require calibration and monitoring of the instrument as a crucial prerequisite for successful retrieval of atmospheric parameters. Calibration applies a sequence of steps to the measurement data while monitoring assesses the optical performance thus permitting degradation corrections. The parameters characterising the instrument were obtained in a sequence of on-ground calibration runs under different environmental conditions. They are stored as *Key Data* and serve as input when deriving calibrated spectra. Relevant calibration steps include the memory effect and non-linearity, wavelength calibration and both spectral and spatial stray light corrections. Since SCIAMACHY is sensitive to the polarisation state of the incoming light, polarisation needs to be thoroughly taken into account. The final step performs the radiometric calibration. Once in orbit, the optical performance monitoring establishes information concerning the channel and wavelength dependent degradation. From the combination of the results for the different light paths, it is even possible to learn how individual optical components degrade.

Keywords: Calibration – Key Data – Calibration Equation – Polarisation correction – Optical performance monitoring

Spaceborne spectral measurements require the translation of measured signals into physical quantities and need to maintain this process with high precision over long time periods. Therefore, calibration and monitoring of the instrument is a crucial prerequisite for any successful retrieval of atmospheric geophysical parameters. Calibration of the instrument has to be valid at any time during the mission. Calibration measurements which cannot be performed in flight need to be obtained before launch on ground. Once in orbit, the instrument is expected to change. It needs to be calibrated in flight where possible, and monitored where in-flight calibration is not feasible.

The goal of the calibration is to convert electronic signals of detectors (Binary Units – BU) into physical units (e.g. W/m^2/nm). This is achieved by applying a complex sequence of individual calibration steps to measurement data. A detailed description of each step can be found in Slijkhuis (2000a) and Lichtenberg et al. (2006). Monitoring aims to give a characterisation of the optical performance as precise as possible in order to correct degradation effects throughout the instrument's lifetime. Therefore, monitoring serves as a general prerequisite for continuous high data product quality. Monitoring related to the optical performance of SCIAMACHY is, to a large degree, linked to the instrument calibration and characterisation status. It establishes in-flight information which permits proper application of on-ground calibration corrections and modelling of the in-orbit environment.

5.1 On-ground Calibration Philosophy

Establishing a valid and accurate on-ground calibration strategy facilitates calibrating the data once the instrument is in orbit. This includes environmental considerations. The experience gained from GOME flying on-board the ERS-2 satellite, where various air-vacuum effects led to calibration problems, showed that spectrometers should ideally be calibrated under thermal vacuum (TV) conditions. In the case of SCIAMACHY, a range of incidence angles on the mirror(s) and mirror-diffuser combinations had to be covered in the calibration, requiring rotation of the instrument. The available vacuum cham-

ber hardware did not allow rotation of the instrument itself, and only provided views in a limited angular range centred on nadir and limb in the flight direction. Therefore, a combination of thermal vacuum and ambient measurements was used. Radiometric sensitivity and polarisation sensitivity of the instrument were measured under TV conditions for *one* reference angle and all necessary instrument modes (limb, nadir and irradiance). The TV on-ground calibration was performed during several campaigns using the OPTEC facility (see chapter 3.5). SCIAMACHY had been placed inside the vacuum chamber with the thermal hardware being replaced by a system based on liquid nitrogen and heaters to reach and maintain the correct temperature. Optical windows in the tank allowed the light from external optical stimuli to enter. In the Key Data (see below), the effect of the optical window had been compensated for. The OPTEC facility was first used for requirement verification tests, i.e. a check to see if the instrument met its requirements. Later, calibration measurements were performed in OPTEC. Since optimising the instrument required major hardware changes, several OPTEC campaigns had to be scheduled and executed. They ran from summer 1997 until spring 2000.

In order to be able to calibrate all incidence angles on the mirrors (or diffusers), component level measurements of all possible mirror combinations and the mirror/ESM diffuser combination were made under ambient conditions. These ambient measurements were performed for a set of angles – including the reference angle measured under TV conditions – and a set of selected wavelengths. From such ambient measurements, the scan angle correction was calculated. The reference angle measurement was used to transfer the results from the ambient measurement to the TV conditions. Measurements included unpolarised and linearly polarised light. The combination of TV and ambient measurements gave the instrument response for all incidence angles at Begin-of-Life (BOL) of the instrument. Implicit assumptions for the combination of the TV and ambient measurements had been that the polarisation dependence of the mirrors and diffusers are the same in air and in vacuum and that there is no temperature dependence. Both assumptions were reasonable for SCIAMACHY because of using uncoated mirrors. Critical points in the transfer of ambient and TV measurements comprised the geometry (incidence angles on the mirrors or diffusers), the illumination conditions and the detector used for the component measurements. Obviously, errors in the geometry would have led to incorrect angle dependence for the calibration quantity to be measured. Light levels during instrument measurements and during component measurements were certainly different. While the footprint of the light source on the component could be matched to the footprint during the instrument measurements, it was impossible to recreate the exact illumination conditions. This could have introduced systematic errors into the calibration. Finally, care had to be taken that the detector used during the measurements under ambient conditions did not introduce artefacts since it differed from the detectors used on-board SCIAMACHY. The ambient calibration was executed between December 1997 and April 1998 in a dedicated set-up, the ARCF (Absolute Radiometric Calibration Facility). In order to allow a rotation of the mirror(s) or the mirror/diffuser combination to any required position, they were placed on a special optical bench. Having two mirrors or a mirror plus a diffuser on the optical bench permitted direct measurement of the combined response of both optical elements and calibration of all SCIAMACHY instrument modes at the appropriate angles. A monochromator and polarisers were used to obtain the response for different wavelengths and polarisations. All measurements took place in a class 100 cleanroom with a controlled temperature of 20°C and 50% air humidity.

In order to minimise potential errors from the measurements performed under ambient conditions, only ratios of measurements were used for the calibration where possible. The individual calibration parameters derived from the on-ground measurements were combined into a set of data files, the *Key Data* files. These Key Data are applied by the data processor to derive calibrated spectra.

5.2 The General Calibration Equation

SCIAMACHY is a scanning instrument measuring only the spatially integrated light of one ground pixel at a time. Tracing the light from the Earth through the telescope, slit, spectrometer, detector, and on-board processing can be described by

$$\vec{I}_{tel}(\lambda,\alpha,\beta) = \mathbf{P_{tel}} * \vec{I}(\lambda, lat, long) \tag{5-1}$$

$\vec{I}$ is the polarised intensity at wavelength λ arriving at the telescope from the geolocation given by *lat*/*long*. $\vec{I}$ is written in Stokes notation as a vector. $\mathbf{P_{tel}}$ is the point spread function of the telescope which may affect the polarisation state of the light, represented here as a matrix. Optical distortion due to the telescope is implicitly included in $\mathbf{P_{tel}}$ which thus may depend on the coordinates α and β. They are defined in the focal plane of the telescope at the entrance slit to the spectrometer part of the instrument. $\vec{I}_{tel}$, the intensity after the telescope, results from a convolution of $\mathbf{P_{tel}}$ and $\vec{I}$ denoted by the operator '$*$'.

After having passed through the telescope, the light crosses the entrance slit where the intensity masked out by the slit is removed:

$$\vec{I}_{slit}(\lambda,\alpha,\beta) = \vec{I}_{tel}(\lambda,\alpha,\beta)\cdot F(\alpha,\beta) \tag{5-2}$$

where F is a function of the focal plane coordinates α and β and is zero where the light is blocked and unity where the light passes unhindered through the slit.

The optics behind the slit project the image of the slit on the detector and add wavelength dispersion to obtain a spectrum. For instruments with an integrating Instantaneous Field of View (IFoV) like SCIAMACHY, the detector can be considered as one-dimensional:

$$I_{det}(x) = \int_{detector} \mathbf{P_0} * \vec{I}_{slit}(\lambda,\alpha,\beta) + B \tag{5-3}$$

where $\mathbf{P_o}$ is the wavelength and polarisation dependent point spread function of the optics, including the dispersion introduced by the spectrometer. The coordinate x is the detector pixel index. Integration is performed over each pixel individually. Possible self-emission of the instrument, i.e. thermal background radiation, is covered by B which may be position dependent. Note that polarisation information is lost once the signal has been projected on the detector.

As soon as the signal is integrated over the detector pixels, it can be treated electronically. Up to this point the signal has been considered purely linear in *intensity*, but the detector material and electronics may introduce non-linearity and hysteresis:

$$S_{det} = E(I_{det}, t_{exp}, I_{det}(t)) \tag{5-4}$$

where E is the function describing the transfer of I_{det} into the digitally sampled detector signal S_{det}, taking into account the exposure time t_{exp}. The function E may depend on the history (memory effect – see below) of I_{det}, represented here as $I_{det}(t)$. Note that in case of SCIAMACHY, on-board processing can modify the digitally sampled signal S_{det} only in the form of co-adding multiple readouts of the detector. Combining all of the equations above, while

- considering a dedicated correction for polarisation sensitivity (see below)
- describing the effects of the point spread function of the optics $\mathbf{P_o}$ on the recorded spectrum as an additive component, and
- introducing explicit temperature dependence of the detector quantum efficiency,

(5-4) can be worked out to

$$S_{det} = I(\lambda)\cdot \Gamma_{inst}(\lambda)\cdot QE(T_{det}, \lambda) + S_{stray} + DC + S_{elec} \tag{5-5}$$

where Γ_{inst} is the total transmission of the instrument, QE the detector temperature dependent quantum efficiency, S_{stray} the stray light, DC the total dark signal and S_{elec} the electronic effects such as non-linearity. This equation must be solved for every detector pixel. In order to obtain the spectrum as a function of wavelength λ for each pixel, the wavelength has to be determined and the equation has to

be inverted to calculate the intensity *I*. Generally, the transmission of the instrument is dependent on the polarisation state of the incoming light.

5.3 Detector Corrections

Several corrections related to the electronics of the detectors and the detectors themselves, i.e. the terms S_{elec} and *DC* in (5-5), have to be applied (see Fig. 5-1). The UV-VIS-NIR channels 1-5 and the SWIR channels 6-8 must be treated separately during the calibration due to their different detector material and readout electronics. Signals are described in terms of Binary Units (BU). The Analogue-to-Digital Converter (ADC) of SCIAMACHY digitises the signal of the detector with 16 bit resolution, meaning that detector signals, also referred to as 'fillings', range from 0 BU to 65535 BU.

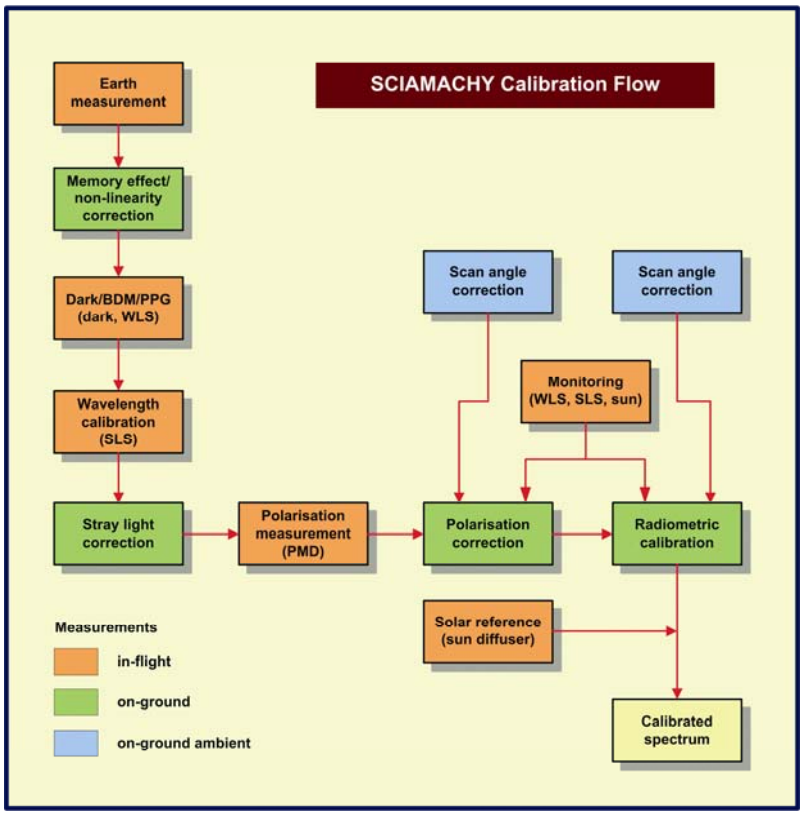

Fig. 5-1: Calibration concept for SCIAMACHY. The final calibrated Earth radiance spectra are obtained by applying several calibration steps to the measured Earthshine signals. They include in-flight calibration measurements (red), on-ground measurements performed under thermal vacuum conditions (green), and component measurements from on-ground ambient tests (blue). The optical performance monitoring (red) provides additional corrections. (Courtesy: SRON)

Channels 1-5 (UV-VIS-NIR)

The first correction to the data is the *memory effect*. The memory effect was discovered in 1996 during an investigation of the linearity of channels 1-5. In a number of measurements covering the range from low detector fillings to saturation, it was found that the signal deviated from a linear response which is defined by a linear fit for all points of up to 90% of the maximum detector fillings (Fig. 5-2). The deviation was independent of the actual signal level, but dependent on the signal level of the *previous* readout (hence the name *memory effect*). Note that the effect depends on the signal level *including* the analogue offset (see below) and dark current. Thus, it has to be applied before any other correction. In order to characterise the memory effect, White Light Source (WLS) measurements followed by several dark measurements were performed on-ground and in-flight. The difference between the first dark measurement after the WLS measurement and subsequent dark measurements gives a correction value

as a function of detector filling. This value needs to be subtracted from the data to correct for the memory effect which is assumed to be the same for all pixels. The total correction for a single readout ranges from -0.61% to 0.21% of the detector filling of the previous readout with a maximum effect at fillings around 19000-21000 BU, depending on the channel. More information can be found in Lichtenberg (2003).

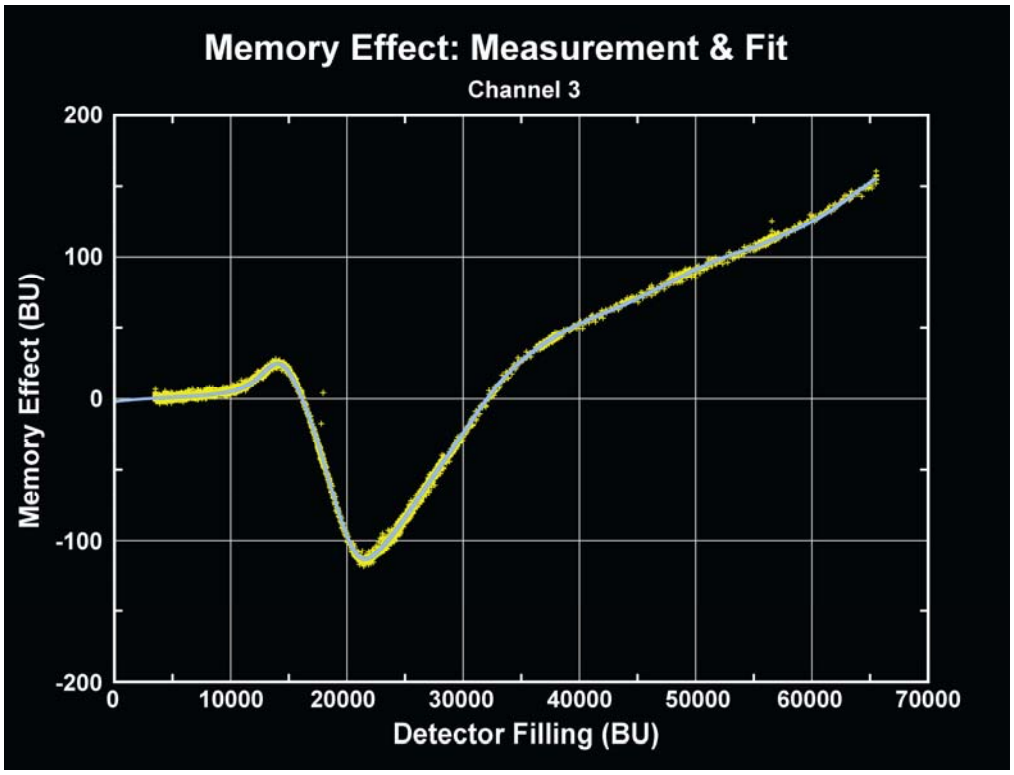

Fig. 5-2: Memory effect for channel 3. Yellow crosses mark the in-flight measurement of the memory effect. The blue solid line is a spline fit through the measurements that is used for the correction. (Courtesy: SRON)

The second detector correction to be applied is the *dark signal* correction. The dark signal is measured in every orbit during eclipse using 5 different states. In channels 1-5, the dark signal consists of two components: the analogue offset (AO) and the leakage current (LC). The analogue offset is independent of exposure time, it is a fixed signal added to the measured signal to avoid negative signals. The leakage current is caused by thermally created electron-hole pairs. The total dark signal for channels 1-5 is

$$DC_{ch15} = f_{coadd} \cdot AO + f_{coadd} \cdot t_{PET} \cdot LC \qquad (5\text{-}6)$$

where f_{coadd} and t_{PET} are the co-adding factor of the cluster and the pixel exposure time, respectively. Note that the analogue offset is only multiplied with the co-adding factor since it is independent of the integration time and is added to the signal for each detector readout. Linear fitting to dark measurements with different integration times yields the in-flight dark signal correction. The dark signal in the UV-VIS-NIR channels is dominated by the analogue offset while the leakage current amounts to only 0.04-0.5 BU/sec and has roughly doubled since launch.

The final detector related corrections concern the *Pixel-to-Pixel Gain* (PPG) and the *detector etalon*. Generally, the pixels in each channel do not show the same response to incoming light. This effect is caused by the electronics and the detector and is thus associated with the individual pixels but not with the wavelength. For channels 1-5, PPG is however small and its correction has turned out to be very stable. The PPG correction used for the UV-VIS-NIR channels had been characterised on-ground. It was derived by first smoothing a WLS measurement, assuming that the spectrum is flat.

Then, the original spectrum was divided by the smoothed measurement, leaving only the high frequency variations that were caused by the different pixel gains in the result.

The etalon correction takes care of in-flight changes of the detector etalon, a spectral structure caused by interference between the boundaries of the protecting SiO layer and the light detecting Si layer. The etalon structures have changed after launch compared to on-ground measurements, perhaps due to contamination on the top layer. The structures also vary with time, particularly after decontaminations. For SCIAMACHY, the detector etalon correction is far smaller than for GOME. It can be derived from in-flight WLS measurements.

Channels 6-8 (SWIR)

The SWIR channels do not suffer from the memory effect. However, these channels display a significant non-linearity, i.e. a deviation in the detector response from a (chosen) linear curve. The non-linearity has been measured during the on-ground calibration campaign and a correction algorithm was defined. The maximum value of the non-linearity is around 250 BU which can be significant for weak absorbers such as CO. A separate non-linearity correction for the channels 6, 6+, 7 and 8 has been derived. Within these channels the non-linearity differs for odd and even pixels (starting pixel numbering with 0) because of the different multiplexers used for these two groups of pixels. Additionally, there is a clear difference in the non-linearity between pixel numbers higher and lower than pixel number 511. This leads to 14 correction curves, four per channel with the exception of channel 6+, which covers only pixels 794 to 1024. Fig. 5-3 shows the non-linearity curves derived for channel 8. The accuracy of the non-linearity correction corresponds to 5-21 BU for detector fillings from 10000-40000 BU, depending on the channel. As for the memory effect correction, the non-linearity has to be corrected before any other correction is applied. More details about the non-linearity can be found in Kleipool (2003).

In addition to the non-linearity, Channels 6+, 7 and 8 contain a significant number of unusable pixels due to the lattice mismatch between the light detecting InGaAs layer and the InP substrate. These channels are doted with a higher amount of Indium (see chapter 3). It changes the lattice constant of the light detecting layer so that it no longer matches the lattice constant of the substrate on which the detecting layer is grown. Any degraded pixels are called ‘bad’ or ‘dead’ pixels. There are various effects making these pixels unusable:

- disconnected pixels preventing any signal readout
- *Random Telegraph* (RT) pixels which spontaneously and unpredictably jump between two levels of dark current leading to different detected signals for the same intensity
- other effects including excessive noise or too high leakage current that saturates the detector

All these effects were measured on-ground and a Bad and Dead Pixel Mask (BDPM) was created. Pixels of the BDPM have to be ignored in any retrieval. As a result of radiation damage to the detectors in orbit, previously sound pixels may become flagged as ‘bad’ or ‘dead’. A dynamic BDPM is determined in-flight based on monitoring and calibration measurements, and updated as pixels change their status. In order to be less affected by noise on the measurements, the dynamic BDPM is smoothed in time.

After the application of the non-linearity and the BDPM, the dark signal has to be corrected. The dark signal correction in channels 7 and 8 is complicated by the presence of a large thermal background BG_{th} and the unforeseen growth of an ice layer on the detector (see chapter 6.4). The ice layer slowly changes the detector temperature and attenuates the signal on the detector, including the thermal background. The dark signal in these channels becomes

$$DC_{ch68} = f_{coadd} \cdot \left(AO + t_{PET} \cdot LC + t_{PET} \cdot \Gamma_{ice} \cdot QE(T_{det}, \lambda) \cdot BG_{th}(\varphi)\right) \quad (5\text{-}7)$$

where Γ_{ice} is the transmission coefficient that changes due to the ice layer and QE is the quantum efficiency for the detector.

For channels 6+ and 8 the quantum efficiency changes with the detector temperature T_{det}, whereas the first part of channel 6 and channel 7 shows no significant temperature dependence. The thermal

background is caused by the thermal radiation of the instrument and is the dominant part of the dark signal (about 4000 BU/sec) in channel 8. It depends on the orbit phase φ because the temperature gradients in the instrument are not completely stable but vary over one orbit due to the changing angle of solar irradiation. The variation of the dark signal over the orbit can reach up to 60 BU/sec which has significant impact on the retrievals of trace gases. In flight, the orbital variation is measured once a month during a dedicated calibration orbit in which only dark signal measurements are performed by looking to deep space at a tangent height of 250 km in limb mode. The variation of the transmission makes the dark signal correction time dependent, meaning that for channels 7 and 8 a dark signal correction calculated from measurements in the same orbit must be used.

The PPG variations in the SWIR channels are larger than in channels 1-5. Differences, although rather stable, of a few percent can be observed. They are monitored on-board but their application is currently not required in data processing (see chapter 8.2). Due to the design of the detectors no detector etalon effect is present in channels 6-8.

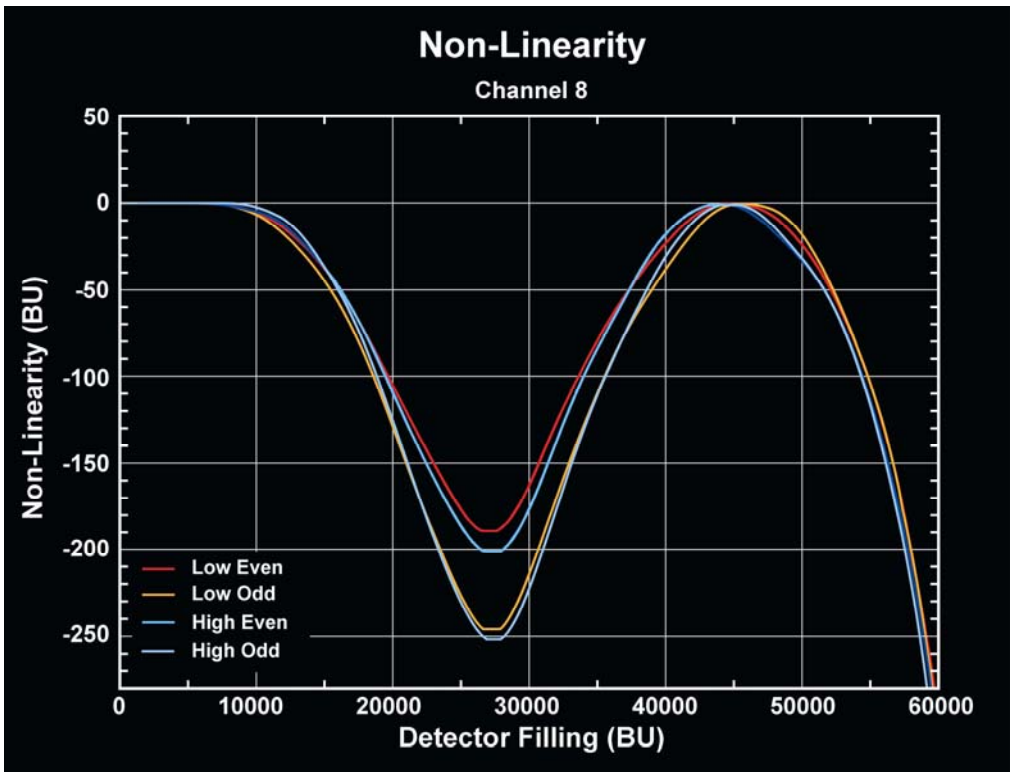

Fig. 5-3: Non-linearity in channel 8 for different pixel regions (indicated by colours). 'Low' pixels are those with pixel numbers below 512. The pixel numbering starts at 0. (Courtesy: SRON)

5.4 Wavelength Calibration

In-flight spectral calibration of SCIAMACHY data uses the internal Spectral Line Source (SLS) measurements with the exception of channels 7 and 8 (see below). For selected lines the Falk algorithm (Falk 1984) determines the pixel positions. These are then fitted to theoretical line positions provided with the calibration data. From the polynomial coefficients of the fit, the wavelength for each pixel can be calculated. Measurements of solar Fraunhofer lines serve as a quality check. In channels 7 and 8, a calibration with the internal SLS lamp is impossible because in these channels not enough useful lines are available to calculate the wavelength calibration with sufficient accuracy. In channel 8 this is caused by bad pixels interfering with the determination of the line position. Channel 7 only contains two strong doublet lines preventing an accurate determination of line positions over the whole channel. In both channels data from on-ground gas cell absorption measurements establish the wavelength calibration.

An additional effect discovered during the on-ground calibration is the *blocking shift*: During the spectral calibration on-ground, the internal SLS and an external SLS were used. A comparison of the measurements done with the two lamps revealed a wavelength shift of up to 0.07 nm. The reason is a partial blocking of the light path during internal SLS measurements. The blocking shift was characterised and is part of the calibration data. Verification of the spectral calibration in flight has proven that SCIAMACHY is spectrally very stable.

5.5 Stray Light

There are two types of stray light, S_{stray} in (5-5), the spectral stray light and the spatial stray light. Both are characterised as a fraction of the total measured intensity for a given pixel.

Spectral stray light is light of a certain wavelength which is scattered to a detector pixel 'belonging' to a different wavelength. It can lead to distortions in the shape of the spectrum. This type of stray light may be caused by a reflection in the instrument after the dispersion of the light beam, or by periodic errors in the spacing of the ruled grooves in a diffraction grating. The source of spectral stray light can be within the same channel, referred to as *intra-channel* stray light, or it can scale with the intensity in a different channel, referred to as *inter-channel* stray light.

Spatial stray light is light entering the telescope from outside the IFoV. It is dispersed just like light from the observation target. Depending on the source of the stray light, the spatial stray light component can add an additional offset to the spectrum and/or distort the spectrum, if the primary source of the stray light has spectral characteristics that differ significantly from the observed target.

Spectral Stray Light

Spectral stray light was characterised on-ground using measurements employing a monochromator. A monochromator produces light in a narrow, predefined spectral band. The centre wavelength of the spectral band can be adjusted. In the derivation of the stray light fractions from monochromator measurements, it is assumed that any signal in detector pixels outside this spectral band is caused by stray light. During the on-ground calibration, the spectral stray light was measured by changing the central wavelength of the monochromator spectral band, thus covering the whole wavelength range of SCIAMACHY. Dividing the integrated light of the monochromator peak(s) by the light detected outside the peak yielded the stray light fraction. The resulting data is part of the calibration data set and is used to correct the spectral stray light in flight.

In a full matrix approach, the spectral stray light determination would measure the stray light contribution from each individual pixel to all other pixels separately. In practice, however, this is not always possible. In the case of SCIAMACHY, a 8192 × 8192 matrix would be needed making the calculation of stray light too slow. Thus, the spectral stray light for SCIAMACHY was initially separated into three types: uniform stray light, ghost stray light and channel 1 stray light. Ghost stray light is caused by a more or less focused reflection of one part of a spectrum to another part of the spectrum. It can distort the shape of the 'true' spectrum, because it does not add signal to all pixels. During the on-ground measurements, many tens of ghost signals were detected in channels 3-8, of which the 20 strongest ones were characterised. The total sum of ghost stray light in a channel is at maximum 1% of the incoming intensity. As it turned out, the split into uniform and ghost stray light did not provide a sufficient correction of the stray light, so the uniform stray light correction was expanded to include a reduced matrix correction.

The reduced stray light matrix describes any of the remaining stray light as a matrix multiplication of an input spectrum and a stray light matrix. A measured spectrum is resampled to lower resolution (1022 pixels instead of 8192), and yields a stray light spectrum of 2048 pixels after matrix multiplication. This stray light spectrum is interpolated to the full 8192 pixel grid and subtracted from the input spectrum.

For channel 1 the situation is less favourable with respect to stray light levels. The on-ground measurements revealed that the spectral stray light in channel 1 can reach levels of up to 10% of the incoming signal for a typical input spectrum. It is also highly wavelength dependent. The main reason for the larger stray light fraction in channel 1 is the high dynamic range of the spectra in this channel, with the lowest signal 3 orders of magnitude smaller than the highest signal. Therefore, a dedicated

method for channel 1, already formulated before launch, combines the correction of uniform and ghost stray light in a modified matrix approach taking polarisation into account. In order to avoid signal-to-noise problems during the spectral stray light measurements, ten wavelength bands were defined separately for x- and y-polarised light leading to a total of 20 bands (see polarisation section below). Characterising intra channel stray light required 9 bands in channel 1 and one band in channels 2-5 for both polarisation directions. The channel 1 detector material is not sensitive for light with wavelengths longer than 1000 nm so the SWIR channels did not need to be considered. For each band the stray light contribution to all detector pixels was calculated leading to a 10×1024 matrix for both polarisation directions. The stray light fraction in channel 1 ranges from less than 1% to as much as 10%. The correction has an accuracy of around 25% and reduces the stray light by an order of magnitude leaving at most 1% stray light in the spectrum after correction.

Spatial Stray Light

Shortly after ENVISAT emerges from eclipse and passes the North Pole, the Sun shines directly into the limb port. In this orbit region spatial stray light cannot be avoided, i.e. the particular effect was foreseen and the data are flagged accordingly. In order to minimise spatial stray light, the ASM is rotated such that the edge of the mirror/diffuser plate points into flight direction, with the diffuser looking to the instrument side during all measurements using the ESM only.

However, both on-ground performance measurements and in-flight limb measurements indicated that there was still a small fraction of spatial stray light present. Dedicated in-flight measurements confirmed the performance measurements and indicated periodic structures in the optics before the slit, resulting in a small fraction of the light being dispersed as by a grating. This has no significant impact for nadir measurements, but limb measurements with a dynamic range of several orders of magnitude over a few degrees do suffer from the spatial stray light. At the moment, no corrections for spatial stray light exist (see also chapter 6.3).

5.6 Polarisation

SCIAMACHY is – like all grating spectrometers without a polarisation scrambler – sensitive to the polarisation of the incoming light, i.e. the response will not only depend on the intensity but also on the polarisation of the light. Thus, polarisation correction is required. It uses the *Mueller matrix* approach (see e.g. Azzam and Bashara 1977, Coulson 1988). Measurements of polarised light can be expressed by a Mueller matrix **M** and a Stokes vector. Since the detectors only yield a single measurement value per pixel, they can be regarded as polarisation insensitive detectors, and any polarisation sensitivity can be included in the Mueller matrix of the optical components between the incoming light and the detector. Thus, only the top row of the end-to-end Mueller matrix of the instrument is relevant, and can be regarded as a polarisation sensitivity vector:

$$S_{det} = \mathbf{M} \cdot \vec{I} \tag{5-8}$$

SCIAMACHY has multiple viewing geometries, selected by appropriate configuration of the scan mirrors and diffusers. Behind the scanner, the Optical Bench Module (OBM) is identical for limb and nadir measurements. The end-to-end Mueller matrix of the instrument can be split up into a Mueller matrix for the scanner, which is configuration dependent, and a fixed polarisation sensitivity vector of the OBM. This yields

$$S_{det} = \left(M_1^{OBM}\ M_2^{OBM}\ M_3^{OBM}\ M_4^{OBM}\right) \cdot \begin{pmatrix} M_{11}^{sc} & M_{12}^{sc} & M_{13}^{sc} & M_{14}^{sc} \\ M_{21}^{sc} & M_{22}^{sc} & M_{23}^{sc} & M_{24}^{sc} \\ M_{31}^{sc} & M_{32}^{sc} & M_{33}^{sc} & M_{34}^{sc} \\ M_{41}^{sc} & M_{42}^{sc} & M_{43}^{sc} & M_{44}^{sc} \end{pmatrix} \cdot \begin{pmatrix} I \\ Q \\ U \\ V \end{pmatrix} \tag{5-9}$$

On the left hand side, a scalar describes the light as detected by the instrument, and on the right hand side, we have the polarisation sensitivity vector $\vec{M}^{OBM}$ of the OBM and the Mueller matrix $\mathbf{M}^{sc}$ defining the response of the scanner to the incoming light represented by another Stokes vector. The first element of this Stokes vector, *I*, denotes the total intensity of the light. *Q* is a measure for the polarisation along the x- or y-axis of a chosen reference frame and can be described as $Q = I_x - I_y$. *U* is a measure for the polarisation along the 45° direction and is defined as $U = I_{45} - I_{-45}$. Finally, V is the circular polarisation component of the incoming light, which is negligible for atmospheric light. Note that the total intensity can be written as $I = I_x + I_y$ or $I = I_{45} + I_{-45}$. Often *Q* and *U* are normalised to the total intensity *I*. We will denote normalised fractions with *q* and *u*.

All $\mathbf{M}^{sc}$ Mueller matrix elements depend on wavelength and on the incidence angle of the light on the scan mirror(s) or diffuser(s). In the calibration, ambient measurements on component level and instrument TV measurements have to be combined meaning that the actual instrument matrix has to be calculated by a multiplication of the matrix for the scanner (combination) and the OBM. Note that though the end-to-end circular polarisation sensitivity of the instrument is irrelevant when V is zero, the scanner may – through its Mueller matrix – cause a circular polarisation component of the light, which requires the circular polarisation sensitivity of the OBM to be known. Although originally not foreseen for on-ground calibration, an update of the calibration concept introduced the circular polarisation sensitivity into the calibration equations. Defining the relative polarisation sensitivity vector of the OBM as

$$\vec{\mu}^{OBM} = \left(1, \quad \mu_2^{OBM}, \quad \mu_3^{OBM}, \quad \mu_4^{OBM}\right) = \left(1, \quad \frac{M_2^{OBM}}{M_1^{OBM}}, \quad \frac{M_3^{OBM}}{M_1^{OBM}}, \quad \frac{M_4^{OBM}}{M_1^{OBM}}\right) \tag{5-10}$$

the response of the instrument to polarised light becomes

$$S_{det} = M_1^{OBM} \cdot \vec{\mu}^{OBM} \cdot \mathbf{M}^{sc} \cdot \vec{I} \tag{5-11}$$

Combination of the polarisation response of the scanner and the OBM using

$$\vec{\mu}^{instr} = \vec{\mu}^{OBM} \cdot \mathbf{M}^{sc} \tag{5-12}$$

and ensuring normalisation of $\vec{\mu}^{instr}$ such that the first element $\vec{\mu}^{instr}$ remains unity, yields the equation describing the instrument response as expressed in total intensity and fractional linear polarisation:

$$S_{det} = M_1^{instr} \cdot I \cdot (1 + \mu_2^{instr} \cdot q + \mu_3^{instr} \cdot u) \tag{5-13}$$

where M_1^{instr} is the radiometric sensitivity of the instrument – with implicit dependence on wavelength for the main science channels, and determined as well for all 7 PMD channels – given by

$$M_1^{instr} = \left| \vec{\mu}^{OBM} \cdot \mathbf{M}^{sc} \right|_1 \tag{5-14}$$

$\vec{\mu}^{OBM}$ is provided in the calibration Key Data as determined from on-ground TV measurements. $\mathbf{M}^{SC}$ can be calculated with a scanner model using as input the actual viewing geometry of the instrument, the complex index of refraction of the mirror material as determined during on-ground ambient calibration and optionally any contamination built up on the scan mirrors since launch.

The term in brackets of (5-13) is the inverse of the polarisation correction factor c_{pol}. It depends on the polarisation sensitivity of the instrument and the polarisation of the incoming light *q* and *u*, assuming a zero circular component (Fig. 5-4). The problem of correcting the response of the instrument for polarisation can thus be divided into two parts: (1) determining the polarisation sensitivity of the instrument and (2) determining the polarisation of the incoming light during the science measurements

in flight. SCIAMACHY exhibits a different sensitivity to different polarisation states of the light. Thus, in the on-ground calibration, measurements with fully linearly polarised light at a range of polarisation angles and with the instrument under thermal vacuum conditions were used to derive the OBM polarisation sensitivities μ_2^{OBM}, μ_3^{OBM}, and μ_4^{OBM}.

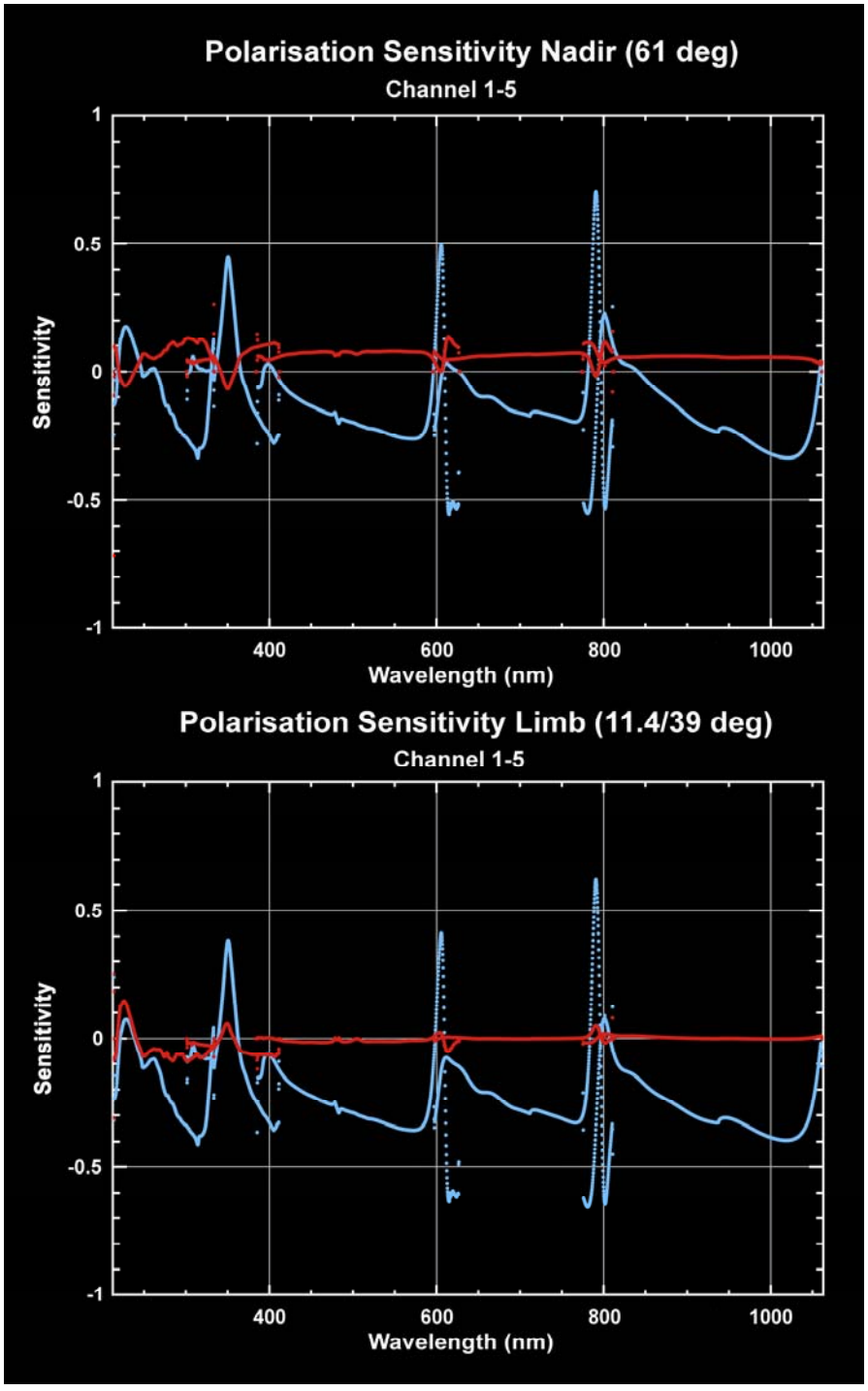

Fig. 5-4: q (blue) and u (red) sensitivity from (5-13) for nadir (elevation angle of 61° top) and for limb (elevation angle of 11.4° and azimuth angle of 39°, bottom) for channels 1-5. Note that these sensitivities are multiplied with the polarisation fractions to get c_{pol} and the correction will thus be smaller than displayed for lower polarisation. (Courtesy: SRON)

The Mueller matrix for the scanner was determined from ambient measurements with fully linearly polarised light with different polarisation directions. Care was taken to ensure that the intensity in all these measurements was the same. With the definitions given above, the polarisation correction factor in terms of on-ground measurements is expressed as

$$c_{pol} = (1 + \mu_2^{instr} \cdot q + \mu_3^{instr} \cdot u)^{-1} \tag{5-15}$$

The second step, the determination of the polarisation of the incoming light is done by determining the ratio of the signal in the PMD channels – which is fully polarised due to the Brewster reflection at the pre-disperser prism (see chapter 3.2) – and the corresponding signal in the science channel for each individual measurement. During calibration this ratio was determined for different directions of linearly polarised light. The comparison of the in-flight ratio with the calibration data gives 7 polarisation values for the whole spectrum, one for each PMD channel. Polarisation values q are calculated from PMD A-F needing the corresponding value of u. The ratio u/q, which depends only on the polarisation angle, is assumed to be constant, such that

$$u_{meas} = q_{meas} \cdot \left(\frac{u}{q}\right)_{const} \tag{5-16}$$

In the original calibration concept, for UV-VIS wavelengths below 600 nm, the polarisation angle from single scattering theory was planned to be used (see below), whereas for higher wavelengths, the ratio u/q from PMD D and PMD 45°, both centred around 850 nm, had to be taken. The values of q and u here are derived by iteration, until the u needed to calculate q from PMD D and the q needed to calculate u from PMD 45° match. In flight, it was noted that PMD 45° delivers signals which are systematically 10-15% higher than expected, even for unpolarised sources such as the Sun. As there are indications that this PMD suffers from stray light, it remains currently unused. Instead, u/q is taken from single scattering theory for the complete wavelength range. From POLDER satellite measurements of u/q this appears to be a sufficiently accurate assumption (Schutgens et al. 2004). Note that for small values of q, this ratio becomes very large, thereby amplifying small measurement errors on q_{meas} into large measurement errors on u_{meas}. However, since the instrument is much more sensitive to q than to u, this has little impact on the radiometric calibration, even though u is notably unreliable. In limb, the calculated polarisation displayed an unexpected drift with increasing tangent height, which is probably due to increasing significance of the spatial stray light contribution as the limb intensity decreases. Therefore, the PMD measurements are only used up to 30 km. Radiative transfer calculations show that above this height, the depolarisation remains constant (Mc Linden et al. 2002) such that for higher limb tangent heights we are able to scale the measured polarisation at 30 km with a value obtained from single scattering theory.

The PMD channels cover only the instrument channels 2-8. For channel 1, the backscattered radiation is dominated by single scattering as can be inferred from radiative transfer calculations. Similarly to the GOME instrument, a theoretical value based on single scattering geometry is used here (Slijkhuis 2000b, Tanzi 1999, Tilstra et al. 2003). The transition region from single scattering to multiple scattering and/or ground reflection in the region between approximately 300-325 nm requires special attention. For GOME, a parameterisation of the degree of polarisation was derived as a function of wavelength (see Balzer et al. 1996), known as the ‘general distribution function’ (GDF) for polarisation. The GDF is characterised by the single scattering value plus three parameters. These parameters are currently obtained using a simplified version of the algorithm from Schutgens and Stammes (2002) where the dependence on scene albedo and ozone content is neglected. More polarisation information may be derived from the channel overlaps of channels 1-6 (five polarisation points) where the different polarisation sensitivities of each channel lead to two independent measurements for the two variables q and u. However, due to calibration inconsistencies, these polarisation points are currently not reliable.

The polarisation values q and u on the level 1b products are specified in an ‘atmospheric’ coordinate frame which is different from the coordinate frame used for the on-ground calibration and Key Data specification. The ‘atmospheric’ coordinate frame is related to the geometry of the scattering of

light in the atmosphere. The choice has been to define *q* as parallel to the local meridian plane – the plane through satellite, zenith, and centre-of-FoV (where its Z axis points in the travel direction of light, i.e. towards the instrument). This plane is depicted in Fig. 5-5 for nadir viewing geometry. For limb viewing geometry, the polarisation plane in the figure is rotated 90° towards the line-of-sight as the line-of-sight is approximately in the flight direction. All derived polarisation values and instrument sensitivities are converted to this 'atmospheric' coordinate frame.

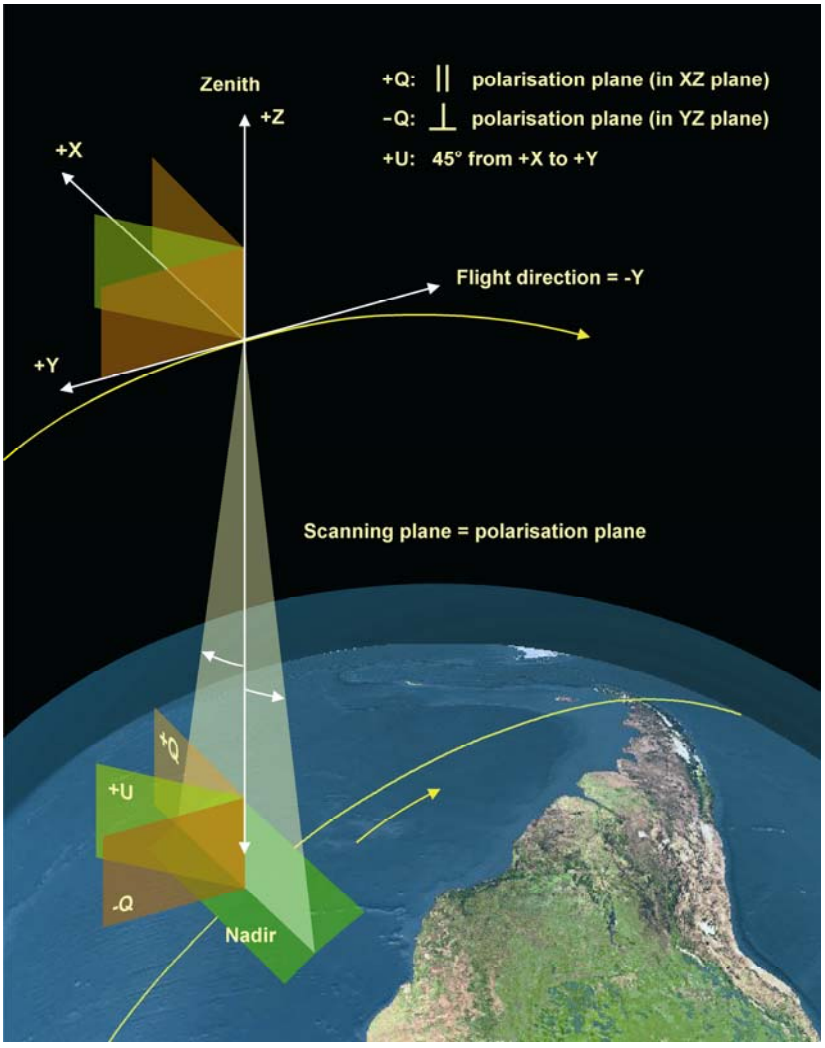

Fig. 5-5: Definition of the nadir coordinate frame used in the output of the data processor for polarisation values q = Q/I, u = U/I. (Courtesy: DLR-IMF)

5.7 Radiometric Calibration

The final step in the calibration of the data is the radiometric calibration. The retrieval of trace gases generally uses the reflectance, the ratio of Earth radiance and solar irradiance. The solar irradiance is measured with on-board diffusers in flight. From (5-13) and (5-15) the reflectance can be written as:

$$R = \frac{\pi}{\mu_0} \cdot \frac{I_{Earth}}{I_{sun}} = \frac{\pi}{\mu_0} \cdot \frac{M_1^{sun}}{M_1^{N,L}} \cdot \frac{S_{det}^{Earth} \cdot c_{pol}}{S_{det}^{sun}} \tag{5-17}$$

$I_{Earth,}$ I_{sun} and S_{det}^{Earth} are the Earth or Sun intensity and the measured signal, μ_0 is the cosine of the solar zenith angle, $M_1^{N,L}$ the instrument radiometric response for limb (*L*) or nadir (*N*) and M_1^{sun} the

instrument radiometric response for Sun diffuser measurements, as calculated from the Mueller matrix for the scanner and the polarisation sensitivity of the OBM. All matrix elements in (5-17) are detector dependent. For a proper calibration the instrument responses have to be determined as a function of wavelength λ and incidence angle α. As mentioned in chapter 5.1, the radiometric response was measured on instrument level under TV conditions, while the mirror and the mirror/diffuser combination were measured under ambient conditions. By combining ambient and TV measurements, it is therefore possible to derive the angular dependence of the instrument throughput, i.e. the Mueller matrix elements. Together with the measured signals S_{det} the reflectance R can be determined from (5-17). Finally, those solar measurements where the neutral density filter is in the light path require correcting. It is done by dividing the recorded signal with the throughput of the NDF.

5.8 Optical Performance Monitoring

One of the main long-term monitoring activities to be performed over the mission's lifetime is to trace the degradation of optical components (Noël et al. 2003). It applies regular trend analyses to measurement data obtained with the internal WLS and of observations of the unobscured Sun above the atmosphere. In order to monitor the different SCIAMACHY light paths, solar measurements are taken in various viewing geometries (Fig. 5-6):

- in limb/occultation geometry (via ASM and ESM mirrors)
- in nadir geometry (via the ESM mirror through the sub-solar port), and
- via the *calibration light path* involving the ASM mirror and the ESM diffuser.

Particularly the WLS produces a rather stable output over time – except for some degradation in the UV – which makes it well suited for throughput monitoring.

In the early phase of the mission the optical performance of the SCIAMACHY instrument was monitored based on the analysis of level 0 data which had been corrected for dead/bad pixels, dark current (fixed value from August 2002), scan angle dependencies, quantum efficiency changes and the seasonally varying distance to the Sun. Meanwhile, the light path monitoring relies on fully calibrated data yielding so called *m-factors* (Bramstedt et al. 2008). The m-factor is defined as the ratio between a measured spectrum of a constant light source – usually the Sun – at a certain time to a spectrum obtained for the same optical path at a reference time. M-factors, therefore, describe how the individual light paths degrade, i.e. they provide the information required for correcting it. For the science channels, m-factors are multiplicative when an absolute radiometric calibration is performed. This is different to the PMD channels where the m-factors impact the polarisation correction in a non-linear fashion.

M-factors are generated for each of the SCIAMACHY light paths (nadir, limb and the calibration light path), taking into account times of reduced instrument performance, e.g. switch-offs or decontamination periods. Moreover, prominent solar features, i.e. Fraunhofer lines used in the derivation of solar data products like solar activity monitoring via the Mg II index, are masked out. For channels 1-6 the m-factors are further spectrally smoothed using a 9 pixel triangular filter to avoid the introduction of additional spectral features in the degradation corrected spectra. The m-factors are operationally produced on a daily grid involving interpolations, if necessary. They can be fed into operational data processing ensuring that the measured signals are fully matched to the performance of SCIAMACHY. Particularly crucial in this context is the calibration of the solar and WLS data used in the m-factor generation, which needs to be consistent with the operational data processing. Therefore, the m-factors are specific for one level 1 product version and thus possibly need to be recalculated after each update of the operational 0-1b data processing software.

From the combination of the results for the different light paths it is possible to derive information about the degradation of individual optical components such as mirrors and diffusers (Fig. 5-6). The degradation of the ASM mirror, for example, may be determined from the ratio of the limb to the nadir light path degradation. To determine the ESM mirror degradation, it is necessary to combine the limb light path results with dedicated measurements involving the extra mirror which is located inside the instrument, only rarely used and thus assumed not to degrade. Finally, the degradation of the ESM diffuser can be computed from the combination of the nadir, limb, and calibration light path. A com-

parison of the limb and nadir light path monitoring results indicates that the major degrading element in the SCIAMACHY optical train seems to be the ESM mirror.

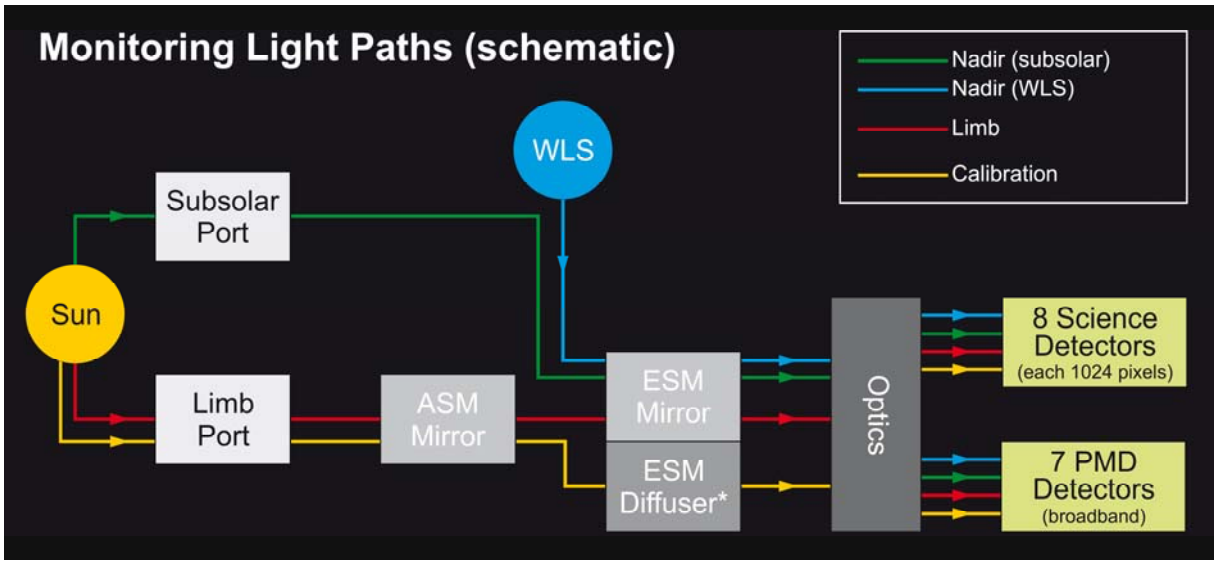

Fig. 5-6: Schematic view of SCIAMACHY light paths used in performance monitoring. (Courtesy: IUP-IFE, University of Bremen)

References

Azzam, R.M.A. and Bashara, N.M. 1977. Ellipsometry and Polarized Light. *Elsevier Science Publishers*, Amsterdam.

Balzer, W., Aberle, B., Loyola, D. and Spurr, R. 1996. GOME Level 0 to 1b Algorithm Description (ER-TN-DLR-GO-0022). *Technical Document*, DLR.

Bramstedt, K. 2008. Calculation of SCIAMACHY M-Factors (IFE-SCIA-TN-2007-01-CalcMFactor). *Technical Document*, IUP-IFE, University of Bremen. Available at http://www.iup.uni-bremen.de/sciamachy/mfactors/mfactor-TN-1-0.pdf

Coulson, K.L. 1988. Polarisation and intensity of light in the atmosphere. *A. Deepak Publishing*, Hampton, VA. USA.

Falk, W.R. 1984. Data Reduction from Experimental Histograms. *Nuclear Instruments and Methods in Physics Research*, 220, 473-478.

Kleipool, Q. 2003. SCIAMACHY: Recalculation of OPTEC 5 Non-Linearity (SRON-SCIA-PhE-RP-013). *Technical Document*, SRON. Available at http://www.sron.nl/index.php?option=com_content&task=view&id=509&Itemid=787&lang=en

Lichtenberg, G. 2003. SCIAMACHY channel 1-5 Memory Effect I: Key data implementation and in-flight measurements (SRON-PhE-RP-11). *Technical Document*, SRON. Available at http://www.sron.nl/index.php?option=com_content&task=view&id=509&Itemid=787&lang=en

Lichtenberg, G., Kleipool, Q., Krijger, J.M., van Soest, G., van Hees, R., Tilstra, L.G., Acarreta, J.R., Aben, I., Ahlers, B., Bovensmann, H., Chance, K., Gloudemans, A.M.S., Hoogeveen, R.W.M., Jongma, R., Noël, S., Piters, A., Schrijver, H., Schrijvers, C., Sioris, C.E., Skupin, J., Slijkhuis, S., Stammes, P. and Wuttke, M. 2006. SCIAMACHY level 1 data: Calibration concept and in-flight calibration. *Atmos. Chem. Phys.*, 6, 5347-5367.

McLinden, C.A., McConnell, J.C., Griffioen, E. and McElroy, C.T. 2002. A vector radiative-transfer model for the Odin/OSIRIS project. *Can. J. Phys.*, 80, 375-393.

Noël, S., Bovensmann, H., Skupin, J., Wuttke, M.W., Burrows, J.P., Gottwald, M. and Krieg, E. 2003. The SCIAMACHY calibration/monitoring concept and first results. *Adv. Space Res.*, 32, 2123-2128.

Schutgens, N.A.J. and Stammes, P. 2002. Parametrisation of Earth's polarisation spectrum from 290 to 330 nm. *J. Quant. Spectr. Rad. Transfer*, 75, 239-255.

Schutgens, N.A.J., Tilstra, L.G., Stammes, P. and Bréon, F.-M. 2004. On the relationship between Stokes parameters Q and U of atmospheric ultraviolet/visible/near-infrared radiation. *J. Geophys. Res.*, 109, D09205, doi:10.1029/2003JD004081.

Slijkhuis, S. 2000a. ENVISAT-1 SCIAMACHY Level 0 to 1c Processing: Algorithm Theoretical Basis Document. *Technical Document*, DLR.

Slijkhuis, S. 2000b. Calculation of Polarisation from Rayleigh Single Scattering (ENV-TN-DLR-SCIA-0043). *Technical Document*, DLR.

Tanzi, C.P. 1999. Considerations on Stokes parameters derived from memo The seventh point polarisation algorithm by P. Stammes. *Internal Report*, SRON.

Tilstra, L.G., Schutgens, N.A.J. and Stammes, P. 2003. Analytical calculation of Stokes parameters Q and U of atmospheric radiation (WR-2003-01). *Scientific Report*, KNMI.